RSC Advances

ROYAL SOCIETY OF CHEMISTRY

www.rsc.org/advances

RSC Advances

RSCPublishing

ARTICLE

Synthesis of high-purity CuO nanoleaves and analysis of their ethanol gas sensing property

Cite this: DOI: 10.1039/xoxxoooooox

Yu Cao[a,†], Shiyu Liu[a,†], Xian Jian[a,†,*], Gaolong Zhu[a], Liangjun Yin[a,*], Le Zhang[a], Biao Wu[a], Yufeng Wei[a], Tong Chen[a], Yuqi Gao[a], Hui Tang[a,*], Chao Wang[b,*], Weidong He[a] and Wanli Zhang[c,*]

Received ooth January 2015,
Accepted ooth January 2015

DOI: 10.1039/xoxxoooooox

www.rsc.org/

CuO nanocrystals with as-designed morphologies such as uniformed quasi-spherical nanoparticles and high-purity nanoleaves were synthesized by adjusting the additions of sodium hydroxide and hydrazine hydrate in aqueous solution at room temperature (25 °C). The increase of sodium hydroxide would accelerate the reaction rate and favor the nucleation of CuO nanocrystals. The decreases of the surface energy will promote the oriented attachment of nanocrystallites along [-111] direction into nanowires and the final formation of two dimension (2D) nanoleaves. Increasing the quantity of hydrazine hydrate could decrease the solution system energy and promote the aggregation of CuO nanocrystals from 2D nanoleaves into 3D quasi-spherical nanoparticles. All the CuO nanocrystals with different morphologies were characterized *via* transmission electron microscope (TEM), field emission scanning electron microscope (FESEM) and x-ray diffraction (XRD). The CuO nanoleaves exhibit an excellent gas sensing performance in responding to ethanol, and performing the strongest response value of 8.22 at 1500 ppm ethanol for ~ 260 °C.

Introduction

Cupric oxide (CuO) has been extensively studied because it exhibits a narrow band gap (1.2 eV) and a number of other interesting properties in catalysts, sensors and lithium ion batteries. For instance, Huang *et al.* have reported the CuO nanosheets with a superior catalytic performance for CO oxidation (47.77 $mmol_{CO}$ $g^{-1}{}_{CuO}$ h^{-1} at 200 °C).[1] Xu *et al.* have revealed the high specific capability and good cycle performance of the CuO mesocrystals.[2] Qin *et al.* have studied the excellent sensing performance in high sensitivity, quick response, and recovery of the H_2S sensor prepared by CuO hollow spheres[3]. Recently, the effectively controlling and adjusting the size, morphology and structure of metal oxide nanocrystals have been advanced remarkably.[4-7] Meanwhile, the morphologies and sizes of CuO directly determined the properties and applications. Hence, many methods have been employed towards the synthesis of various structures, for instance, thermal oxide,[8] wet chemical method,[9] electrochemical method,[2] pulsed wire explosion,[10] and chemical vapor deposition (CVD).[11] And the structures such as ribbons, platelets, spheres, flowers, hollow structures and so on, have been synthesized successfully.[12-16]

Although investigations have been focused on exploring synthetic methods, it is still a crucial and fascinating problem to adjust numerous nanostructures with a simple method.[17-19] In order to modulate numerous nanostructures with a simple method, great efforts of the structure of metal oxide have been investigated. To classify these modulating approaches, it could be mainly divided into choosing various synthetic approaches, several parameters of the growth process and different kinds of protected reagents.[20-23] Recently, some new approaches have been reported. For instance, Ghosh *et al*. synthesized mesoporous cube-shaped CuO with a multishell microcarpet-like patterned interior *via* a facile aqueous-based process using copper nitrate, oxalic acid, and phosphoric acid in TBC.[24] Huang *et al*. provided the method to tune the reaction kinetics by metal cations such as Zn^{2+}, Ag^{+} and Al^{3+}.[1] The researches and the creations of approaches for controlling the structures of metal oxide greatly enrich the field of nanoscience and nanotechnology.

In this work, we have reported a facile method for modulating diversity structures of CuO nanocrystal such as high-purity nanoleaves, uniformed quasi-spherical nanoparticles and fine nanoparticles in aqueous solution *via* mixing and tuning the additions of copper chloride, sodium hydroxide and hydrazine hydrate without other surfactants at room temperature (25°C). A series of experiments are carried

out to perform the changes of various morphologies. The mechanism of the whole synthesis process is revealed by the analysis of reaction kinetics and an oriented attachment growth step. We found that a quick reaction rate would favor the nucleation of CuO nanocrystals, which promote the decrease of the surface energy and the self-assembly of CuO nanocrystallites into nanowires along the [-111] direction, and the final formation of CuO nanoleaves from nanowires perpendicular to the [-111] direction. The hydrazine hydrate could eliminate the nanocrystals energy, decrease the reaction barrier and obviously shorten the reaction time from 40 h to 8 h and decrease the reaction temperature from 80°C to 25°C. [25, 26] The response to testing gas at different concentrations of ethanol in various temperatures was taken as a case to demonstrate the well performance of the CuO nanoleaves-base sensor. The response to ethanol is close to those of gas sensor report recently.[27] Further experiments and studies had been carried out and demonstrated that CuO nanoleave-based sensor displays the strongest response of 8.22 at 1500 ppm ethanol in 260 °C. The well property in sensing ethanol may be attributed to the 2D structure of CuO nanoleaves. The purified and uniformed CuO nanostructures synthesized by the facile aqueous solution method may have an extensive application in catalysts, lithium ion batteries and solar cells.

Experimental

Synthesize the quasi-spherical nanoparticles and nanoleaves

All reagents in this experiment were analytical grade and used without further purification. In a typical experiment, 1 mmol of $CuCl_2 \cdot H_2O$ was firstly dissolved in 300 ml deionized water under a constant magnetic stirring at room temperature (25 °C). Blue precipitates appeared quickly after X mmol NaOH (0.2 mol/L) added into $CuCl_2$ solutions. Then, a total of hydrazine hydrate (0.1mol/L) with the additions of Y mmol was added into the above solutions. The resultant solutions turned into light yellow in a short time and finally changed into grey in a longer period of ~8 h. The precipitates of each sample were washed more than three times with deionized water and ethanol. Finally, the products were filtered and dried at 100 °C for 3 h in the drying oven. The morphologies of as-prepared products were modulated from nanoparticle to nanoleaves when the values of X range from 3.2~4.8 mmol while the value of Y is 0.4 mmol and the morphologies were modulated from nanocubics twined with nanoleaves to nanoparticled when the Y range from 0.4~2.0 mmol while the value of X is 3.4 mmol.

Gas Sensor Preparation

The as-prepared CuO (the value of X and Y is 4.0 and 0.4 mmol, respectively) was initially grinded with deionized water into grey slurry and coated uniformly upon an alumina ceramic tube printed with a pair of Au electrodes at the two ends. The CuO-coated substrate was dried in the air for ~3 h and then annealed at 500 °C for ~2 h. A Ni-Cr alloy wire as a resistance heater was inserted into the ceramic tube to provide the working temperature for the gas sensor. The electrical and ethanol sensing performances of as-prepared CuO were detected by a measurement system of WS-30A (Zhengzhou Winsen Electronic Technology Co. Ltd., China)

Characterizations

The size and morphology of Cu nanocrystals were observed with a JSM-7600F field emission scanning electron microscope (FESEM; JEOL, Ltd, Tokyo, Japan) and a JEM 2100F transmission electron microscope (TEM; JEOL, Ltd, Tokyo, Japan) with an operating voltage of 200 kV. X-ray diffraction (XRD) patterns were recorded on an X-ray diffractometer (XRD-7000; Shimadzu, Cu Kα, λ = 0.154178 nm).

Results and discussion

Figure 1 describes the typical synthetic process of various CuO nanocrystals in aqueous solution with constant magnetic stirring at room temperature (25 °C) for 8 h. By adding different additions of NaOH (X mmol, 0.2 mol/L) and hydrazine hydrate (Y mmol, 0.1 mol/L), CuO fine nanoparticles, high-purity nanoleaves and quasi-spherical nanoparticles were obtained.

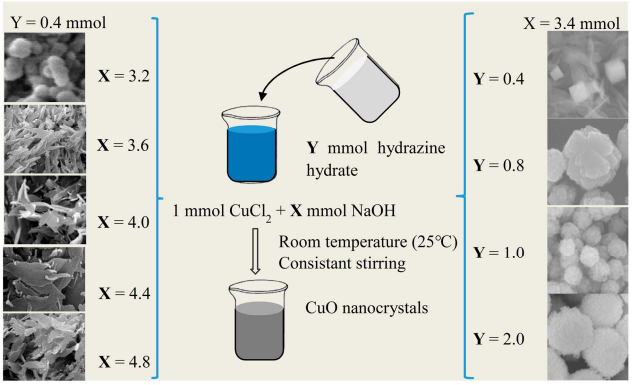

Figure 1. Scheme illusion of the synthetic process of various CuO nanocrystals by adjusting the additions of NaOH (0.2 mol/L) and hydrazine hydrate (0.1 mol/L).

Adjusting CuO morphologies with hydrazine hydrate

Various CuO nanocrystals were prepared by changing the additions of hydrazine hydrate when the NaOH solution was 3.4 mmol. **Figure 2** shows the scanning electron microscope (SEM) images of the as-prepared products when the additions of hydrazine hydrate range from 0.4 to 2.0 mmol. From the SEM observation, various CuO nanocrystals including nanoleaves accompanied with nanocubics, irregular nanoparticles and uniformed quasi-spherical nanoparticles were prepared. In the sample prepared at 0.4 mmol hydrazine hydrate, CuO nanoleaves and nanocubic formed in this case. The length of CuO nanoleaves are ~600 nm and the width of CuO nanocubics are ~350 nm on average. With the addition of hydrazine hydrate up to 0.8 mmol, the as-prepared CuO nanocrystal displayed irregular shapes, and their sizes ranged from 400 nm to 1400 nm and ~770nm on average (**Figure 2**a). When the hydrazine hydrate addition increased to 1 mmol, uniformed CuO nanoparticles sized about 500 nm were prepared (**Figure 2**b). The CuO nanoparticles got more round,

uniform and larger in size (~1080 nm) in the case of 2.0 mmol hydrazine hydrate (**Figure 2**d, 3c). From the SEM observation, it is obvious that the increasing quantity of hydrazine hydrate has a significant influence on modulating the morphologies of CuO nanocrystals ranging from two-dimension (2D) to three-dimension (3D). Large quantities of hydrazine hydrate favour the agglomeration of CuO nanoparticles into quasi-spherical nanoparticles and results in the larger size of as-prepared nanoparticle.

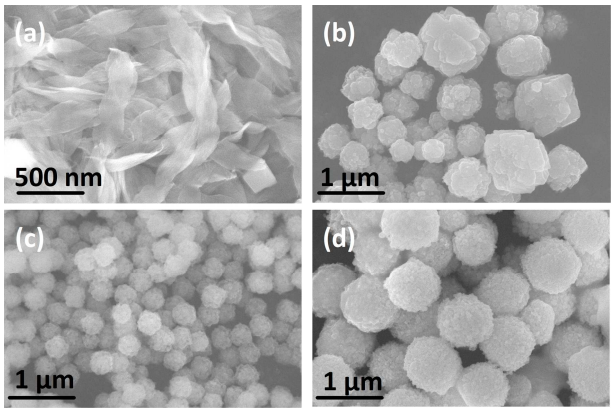

Figure 2. SEM images of CuO nanocrystals under different molar ratio of hydrazine hydrate (0.1mol/L): (a) 0.4 mmol, (b) 0.8 mmol, (c) 1.0 mmol, (d) 2.0 mmol.

Adjusting CuO morphologies with NaOH

Typical spherical nanoparticles have been well studied in depth,[28, 29] while as a novel and basical structure, nanoleaves and its potential applications have been advanced remarkably.[30-32] In order to prepare high-purity CuO nanoleaves, the other parameters that affect the shape of product is further considered and designed carefully. The additions of NaOH are controlled when the addition of hydrazine hydrate is 0.4 mmol. The morphologies of these samples produced at room temperature are displayed in **Figure 3**. We found that in the case of 4.0 mmol NaOH, high-purity CuO nanoleaves were obtained successfully.

Figure 3a shows the SEM image of as-obtained CuO fine nanoparticles obtained when the addition of NaOH is 3.2 mmol. The smaller crystallite size of CuO nucleus firstly formed, and then assembled, finally aggregated to form CuO fine nanoparticles. As shown in **Figure 3**b, when we increase the addition of NaOH to 3.6 mmol, plenty of incomplete CuO nanoleaves mixed with few CuO nanocubics and flowerlike CuO nanostructures are produced. **Figure 3**c-d clearly shows the uniformed high-purity CuO nanoleaves without other shapes as increasing the addition of NaOH to 4 mmol. These CuO nanoleaves, which perform well 2D nanostructure, are flat and stretched with the length, width and thickness of 600-900 nm, 250-300 nm and 10-20 nm, respectively. Uniform high-purity CuO nanoleaves would exist steadily and tend to aggregate with each other as the additions of NaOH increase to 4.4 and 4.8 mmol (**Figure 3**e-f).

The SEM observation confirms that the morphologies of CuO were modulated from fine nanoparticles to nanoleaves with increasing the amount of NaOH from 3.2 to 4.8 mmol. Furthermore, increasing quantity of NaOH favors the nucleation of CuO and the growth of high-purity CuO nanoleaves, might due to the enhancement of the interaction between OH^- and copper ions.

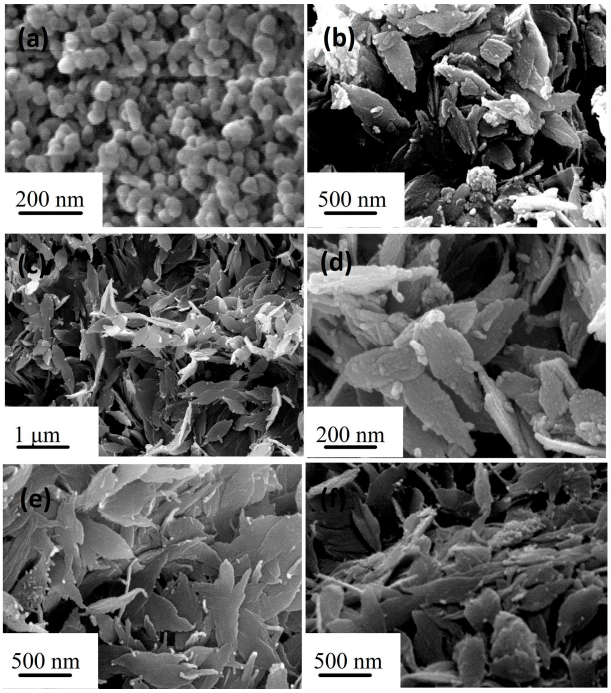

Figure 3. SEM images of CuO nanocrystals prepared adjusting the molar ratio of NaOH into (a) 3.2 mmol, (b) 3.6 mmol, (c, d) 4.0 mmol, (e) 4.4 mmol and (f) 4.8 mmol.

Structure characterization of CuO nanoleaves

From the XRD patterns of CuO nanoleaves and quasi-spherical nanoparticles (**Figure 4**), it is evident that these patterns could be indexed to the pure monoclinic CuO (space group Cc; a=4.689 Å, b=3.420 Å, c=5.130 Å, β=99.57°; PDF 01-089-5899) and no other phases were found. The most strong peaks with 2θ values of 35.558 and 38.759 correspond to (-111) and (111) crystal plane of monoclinic CuO, respectively. It is suggested that after the nucleation of monoclinic CuO, the solution systems are benefit to the growth of (-111) and (111) crystal plane. The crystallite size of CuO for the most intense peak (-111) plane was determined from the X-ray diffraction data employing the Debye-Scherrer formula:

$$D = \frac{k\lambda}{\beta \cos\theta}$$

Where D is the crystallite size, k = 0.89 is a correction factor to account for particle shapes, β is the full width at half maximum (FWHM) of the most intense diffraction peak (-111) plane, λ = 1.5406 Å is the wavelength of Cu target, and θ is the Bragg angle. The average crystallite sizes of the as-product CuO powders are calculated as 19.69, 18.44 and 14.22 nm while the molar addition of NaOH is 4.0, 4.4 and 4.8 mmol, respectively.

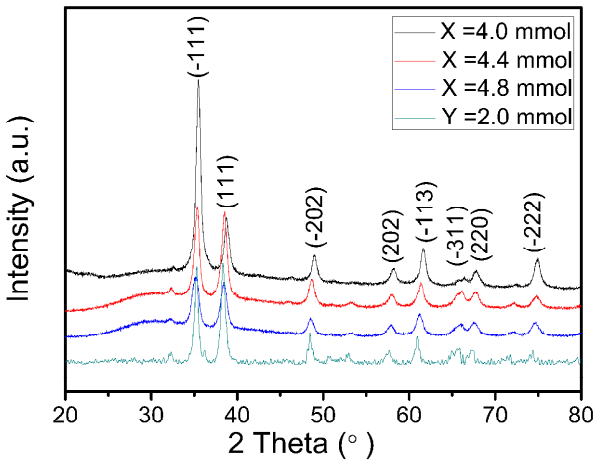

Figure 4. XRD pattern of the CuO nanoleaves prepared of 4.0, 4.4 and 4.8 mmol NaOH (0.2 mol/L) within 0.4 mmol hydrazine hydrate (0.1mol/L) and quasi-spherical nanoparticles prepared of 2 mmol hydrazine hydrate (0.1mol/L) within 3.4 mmol NaOH (0.2 mol/L) at room temperature by constant stirring for 10 h.

It means that the CuO nanoleaves contain a numerous of CuO nanocrystallites, which is in agreement with the observation of HRTEM images.

TEM images of high-purity CuO nanoleaves as the addition of 4.0 mmol NaOH are shown in **Figure 5**a, the flowerlike shape is mainly because the overlapping of different CuO nanoleaves. Small crystallite particles with a diameter of about 18 nm (**Figure 5**b-c) are observed, the result is in agreement with the calculation of Debye-Scherrer formula. Needlelike CuO nanowires composed of many small particles assemble with each other, the length of these nanowires range from 350 to 950 nm, while the width of these nanowires range from 10 to 50 nm (**Figure 5**a-c). **Figure 5**d shows the HRTEM image of one nanoleaf originating from the marked area in **Figure 5**b. A clear and continuous lattice-fringe indicates that the CuO nanoleaves share the same crystallographic orientation. The small crystallites composing to CuO nanoleaves are monocrystalline with the interfringe distance of 0.25 nm corresponding to the (-111) plane of monoclinic CuO, which is in agreement with the results of XRD pattern. A Fast Fourier Transformation (FFT) pattern originating from marked area in **Figure 5**d reveals that the high-purity CuO nanoleaves have the same crystallographic orientation. From the above analysis, it is evident that the needlelike CuO nanowires perpendicular to the [-111] direction to form high-purity CuO nanoleaves, the needlelike CuO nanowires were formed by the assembly of CuO nanoparticles along [-111] direction with the perfect crystallographic orientation of (-111), and oriented attachment goes through these entire course.

The EDX result demonstrates the existence of Cu and O elements, and the atomic ratio of Cu:O is 48.88:51.12, indicating the high-purity of as-prepared CuO nanoleaves (Figure S1 and Table S1 in the Electronic Supplementary Information‡). The UV–vis spectrum of the as-obtained CuO nanoleaves well dispersed in ethanol shows a broad absorption peak centered at ~278 nm. The band gap of CuO nanoleaves can be determined *via* UV-vis spectrum by employing Tauc/Davis-Mott Model.[33] The direct band gap energy of the as-obtained CuO nanoleaves is calculated to be 2.17 eV (Figure S2).

Growth mechanism of CuO Nanocrystal

The chemical reaction of the overall synthetic process is assumed as follows:

$$Cu^{2+} + 2OH^- \Leftrightarrow Cu(OH)_2 \downarrow \quad (1)$$

$$Cu(OH)_2 \xrightarrow{\text{hydrazine hydrate}} CuO + H_2O \quad (2)$$

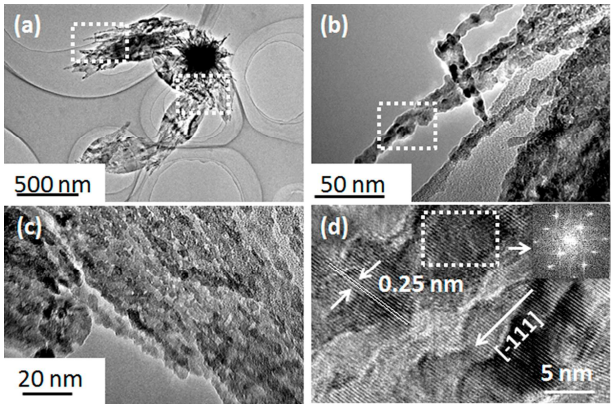

Figure 5. Morphology of the high-purity CuO nanoleaves (X = 4 mmol), (a) low magnification TEM image, (b) TEM image of CuO nanowires, (c) TEM image of well-aggregated CuO nanoleaves, (d) HRTEM image of as-prepared CuO nanoleaves and the corresponding fast Fourier transform (FFT) patterns.

It is suggested that the synthetic process goes through two steps to form CuO. The first step is the formation of a metastable phase of light blue $Cu(OH)_2$ in a short period which is easily to transforms into more stable CuO.[34] Due to the reversibility of the first step, the increase of the OH^- concentration may accelerate the reaction rate. What's more, the low solubility product (*K*sp) is -19.32 for $Cu(OH)_2$, which indicates that the acceleration of the forward reaction rate and the low supersaturated degree favor the nucleation and the growth of $Cu(OH)_2$. The second step is the dehydration and condensation of $Cu(OH)_2$, and the formation of CuO nanocrystals. Compared with Xu's experiments in the preparation of CuO nanoleaves at 35°C for 40 h by adjusting the pH=12,[26] our experiments are more facile by employing hydrazine hydrate agent at 25°C for 8 h. The colour of the suspension changed from light yellow into grey, which indicates the second reaction process may include the reduction and oxidation of copper ions. Since the solubility of CuO is much less than that of $Cu(OH)_2$, the transition from $Cu(OH)_2$ to CuO could decrease the free energy of the reaction system. In this case, it is suggested that the hydrazine hydrate decreases the reaction barrier of the formation of CuO and has the function of driving the second step faster. From the above analysis, the precursor $Cu(OH)_2$ is firstly prepared by the mixing of $CuCl_2$ and NaOH solutions, and the low

supersaturated degree of $Cu(OH)_2$ in aqueous solution and the high concentrations of OH^- favor the nucleation and the growth of $Cu(OH)_2$. The CuO nanocrystals are finally prepared by the dehydration of $Cu(OH)_2$ and the hydrazine hydrate promote this process to accelerate the transition and cut downs the transition time, which may open a novel field by adjusting the morphology in controlling the reaction kinetics.

It is further found that the Gibbs Free Energy (GFE) decreases with the shape factor and increases with decreasing of particle size.[35] With the increasing sizes of the spherical nanocrystal, the GFE decreases and the stability of the CuO nanoparticles increase. It indicates that the increase of the addition of hydrazine hydrate may achieve the elimination of the GFE of reaction system and modulate 2D nanoleaf to 3D spherical morphology of lager CuO particles sized of ~1080 nm.

Summarily, the increase of the additions of NaOH favors the nucleation of CuO and the growth of CuO nanoleaves. Meanwhile, the tendency of the surface energy decreasing of smaller CuO nanoparticles drives the assembly along [-111] direction with the perfect crystallographic orientation of (-111) into needlelike CuO nanowires, and needlelike CuO nanowires perpendicular to the [-111] direction to form high-purity CuO nanoleaves (as shown in **Figure 6**). Oriented attachment goes through entire course.

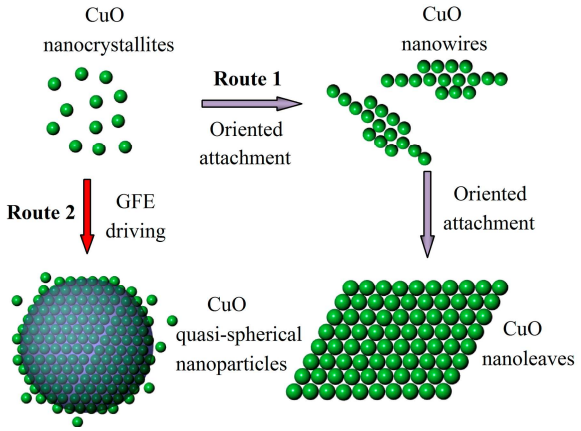

Figure 6. Scheme of the growth of CuO nanoleaves and CuO nanoparticles under different conditions.

Ethanol Gas sensing performance

The response (the ratio of the resistance of sensor, R_{gas}/R_{air}) and recover properties of the CuO nanoleaf-based sensor at different temperatures, concentration is investigated by using ethanol as a targeted gas analyte. In order to study the best operating temperature for sensing ethanol, the response at different temperatures under the concentration of 1500 ppm of ethanol is investigated. **Figure 7**a shows the response of the CuO nanoleaf-based sensor at the concentration of 1500 ppm of ethanol, with the increase of the testing temperature from 100 to 370 °C, the response curve increases at initial stage and has the maximum value at 260 °C, and decreases finally. It indicates that the best operating temperature for sensing ethanol is about 260 °C. **Figure 7**b shows the response curves of the CuO nanoleaf-based sensor with the concentrations of ethanol at the range of 50~1500 ppm at 260 °C. The response curve increases continuously with the concentration of ethanol increasing from 50 to 1000 ppm, and the sensing response of ethanol becomes saturated when the concentration is higher than 1500 ppm. The minimum response of ethanol is ~1.38 at 260 °C at concentration of 10 ppm ethanol.

Figure 8 demonstrates the response and recovery curves of CuO nanoleaf-based sensor to ethanol of which concentrations range from 50 to 1500 ppm at 260 °C. The resistance values increase sharply when CuO nanoleaf-based sensor is exposed to ethanol, while the resistance values decrease quickly when the ethanol is removed. The responses/recover time (the time required to reach 90% of the equilibrium value of resistance) is about 23-55 s and 20-57 s, respectively. The CuO nanoleaf-based sensor displays a sensitive response to ethanol at a low testing temperature and ethanol concentration. It is mainly because of the small size and 2D structure of CuO nanoleaves.

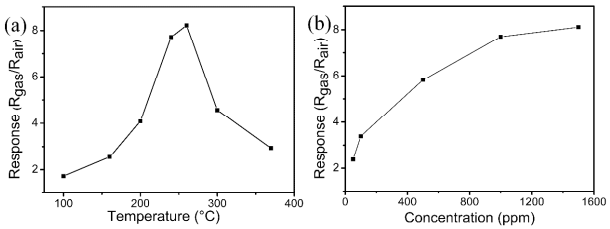

Figure 7. (a) Relationship of the testing temperature versus response to ethanol of CuO nanoleaf-based sensor under 1500 ppm ethanol. (b) Relationship between the concentration and the response to ethanol of CuO nanoleaf-based sensor at 260 °C.

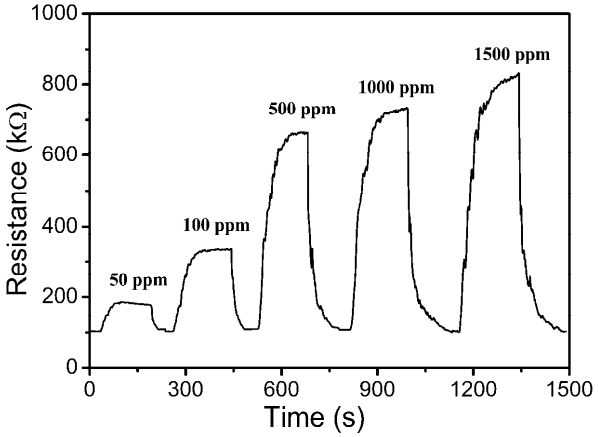

Figure 8. Response and recovery curves of CuO nanoleave-based sensor toward different concentrations of ethanol at 260 °C.

It is well known that the adsorption and desorption of testing gas on the surface of CuO-based gas sensor attribute to the changes of electric resistance and directly lead to the response to the testing gas. As a p-type semiconductor, the resistance of CuO-based gas sensor increases when it is exposed into the testing gas (ethanol) and then decreases when it is exposed into air. Herein, the chemical reaction of the C_2H_5OH upon the

surface of CuO nanoleaves at 100-370 °C is assumed as follows:[27, 36, 37]

$$C_2H_5OH(ads) + 3O_2^-(ads) \rightarrow 2\,CO_2(g) + 3H_2O(g) + 3e^-(3)$$

The formation of O_2^- (ads) is attributed to the adsorption of oxygen molecules to the surface of CuO nanoleaves. At less than 240 °C, the ethanol molecules without enough energy don't react with the O_2^-(ads) on the surface of CuO nanoleaves resulting in the lower sensitivity of CuO gas sensor. With the increase of temperature to 240 °C, the adsorbed oxygen molecules change from O_2^- (ads) to O^- (ads), and the thermal energy of CuO gas sensor is high enough to maintaining the react activation energy. On the other hand, the adsorption of ethanol molecules on the surface of CuO nanoleaves turns to be difficult and some ethanol molecules may react with the oxygen in the air, which leads to the dropped response when the operating temperature is more than 260 °C. The sensor behavior is similar to the case of CO gas in the CuO sensing device reported by Chang *et al*.[38] In this case, the electrons from valence band of CuO are trapped *via* oxygen which leads to the accumulation of holes and the increase of carrier's concentration. When the CuO nanoleaf-based sensor is exposed into the testing gas (ethanol), the production of electrons would neutralize and decrease the amount of holes, resulting in the sharp increase of the resistance. Compared with that reported by Wang's[39], the response to ethanol of CuO nanoleaf-based sensor is more sensitive and strong. Repeated testing have been carried out during twenty days and the response for ethanol of the CuO nanoleaf-based sensor has no significant variation, which indicates the well stability of the CuO nanoleaf-based sensor.

The significant various in response to ethanol may be attributed to the 2D structure advantages of CuO nanoleaves, of which promote the diffusion and adsorption/desorption of ethanol molecules upon the nanoleaves. The well conductivity of the quasi single crystal of CuO nanoleaves prepared in aqueous solution through the oriented attachment can facilitate the transportation of holes carriers in the sensing process. All of these elements directly favor the well performed sensing response of ethanol. The 2D structure of CuO nanoleaves provide a new choice for the application in gas sensor and CuO nanoleaf-based sensor may have potential application in detecting ethanol in low concentration at low temperature, further investigations will be carried out.

Conclusions

The morphology of CuO nanocrystal could be modulated simply by adjusting the ratio of sodium hydroxide and hydrazine hydrate, the uniformed CuO nanoparticles and high-purified CuO nanoleaves are obtained in control. Increasing the usage of sodium hydroxide will modulate the morphology of CuO from fine nanoparticle to high-purity nanoleaves and favor the acceleration of the reaction rate and the nucleation of CuO nanocrystal. The decreases of the surface energy will promote the oriented attachment of nanocrystallites into nanowires and the final formation of 2D nanoleaves. Increasing the quantity of hydrazine hydrate could decrease the solution system energy and promote the aggregation of CuO nanocrystals from 2D nanoleaves into 3D nanoparticles. The 2D CuO nanoleaves exhibit excellent gas sensing performance in responding ethanol. CuO nanoleaf-based sensor displays the strongest response of 8.22 at 1500 ppm ethanol in 260 °C. This work provides a facile and effective method in modulating CuO morphology including uniformed CuO nanoparticles and high-purity CuO nanoleaves, and the well sensing prosperity of CuO nanoleaves to ethanol. The as-prepared CuO nanostructures may have great potential applications in the field of catalyst, lithium ion batteries and solar cells.

Acknowledgements

This work was supported by the National Natural Science Foundation of China (Grant No. 51202228, 51302029, 51402040, 51402045), the Open Foundation of State Key Laboratory of Electronic Thin Films and Integrated Devices (KFJJ201411) and the National Hi-Tech Research and Development Program (863 Program) of China (No. 2015AA034202).

Notes and references

[a] Clean Energy Materials and Engineering Centre, School of Energy Science and Engineering, State key Laboratory of Electronic Thin Films and Integrated Devices, Centre for Information in Biomedicine, University of Electronic Science and Technology of China, Chengdu, 611731, China.

[b] Laboratory of Precision Manufacturing Technology, Institute of Machinery Manufacturing Technology, China Academy of Engineering Physics, Mianyang, 621900, China

[c] State key Laboratory of Electronic Thin Films and Integrated Devices, Insitute of Microelectronic & solid-state electronics, University of Electronic Science and Technology of China, Chengdu, 610054, China.

* Corresponding Author: Emails: jianxian20033835@163.com, tanghui@uestc.edu.cn, wangchaohit@126.com and wlzhang@uestc.edu.cn

† These authors contributed the equally to this work.

‡ Electronic Supplementary Information (ESI) available: See DOI: 10.1039/b000000x/

1. H. Huang, L. Zhang, K. Wu, Q. Yu, R. Chen, H. Yang, X. Peng and Z. Ye, *Nanoscale*, 2012, **4**, 7832-7841.
2. M. Xu, F. Wang, B. Ding, X. Song and J. Fang, *RSC Advances*, 2012, **2**, 2240-2243.

3. Y. Qin, F. Zhang, Y. Chen, Y. Zhou, J. Li, A. Zhu, Y. Luo, Y. Tian and J. Yang, *The Journal of Physical Chemistry C*, 2012, **116**, 11994-12000.
4. R. S. Devan, R. A. Patil, J. H. Lin and Y. R. Ma, *Advanced Functional Materials*, 2012, **22**, 3326-3370.
5. Z. Wang and L. Zhou, *Advanced materials*, 2012, **24**, 1903-1911.
6. G. Shen, P.-C. Chen, K. Ryu and C. Zhou, *Journal of Materials Chemistry*, 2009, **19**, 828-839.
7. R. Sui and P. Charpentier, *Chemical reviews*, 2012, **112**, 3057-3082.
8. M. Kaur, K. Muthe, S. Despande, S. Choudhury, J. Singh, N. Verma, S. Gupta and J. Yakhmi, *Journal of Crystal Growth*, 2006, **289**, 670-675.
9. H. Zhu, D. Han, Z. Meng, D. Wu and C. Zhang, *Nanoscale research letters*, 2011, **6**, 1-6.
10. S. Krishnan, A. Haseeb and M. R. Johan, *Journal of nanoparticle research*, 2013, **15**, 1-9.
11. D. Barreca, E. Comini, A. Gasparotto, C. Maccato, C. Sada, G. Sberveglieri and E. Tondello, *Sensors and Actuators B: Chemical*, 2009, **141**, 270-275.
12. H. Hou, Y. Xie and Q. Li, *Crystal growth & design*, 2005, **5**, 201-205.
13. D. Li, Y. Leung, A. Djurišić, Z. Liu, M. Xie, J. Gao and W. Chan, *Journal of crystal growth*, 2005, **282**, 105-111.
14. J. Zhang, J. Liu, Q. Peng, X. Wang and Y. Li, *Chemistry of materials*, 2006, **18**, 867-871.
15. X. Wang, C. Hu, H. Liu, G. Du, X. He and Y. Xi, *Sensors and Actuators B: Chemical*, 2010, **144**, 220-225.
16. J. C. Park, J. Kim, H. Kwon and H. Song, *Advanced Materials*, 2009, **21**, 803-807.
17. T. R. Gordon, M. Cargnello, T. Paik, F. Mangolini, R. T. Weber, P. Fornasiero and C. B. Murray, *Journal of the American Chemical Society*, 2012, **134**, 6751-6761.
18. J. U. Park, H. J. Lee, W. Cho, C. Jo and M. Oh, *Advanced Materials*, 2011, **23**, 3161-3164.
19. B. Liu, W. Zhang, F. Yang, H. Feng and X. Yang, *The Journal of Physical Chemistry C*, 2011, **115**, 15875-15884.
20. A. J. Houtepen, R. Koole, D. Vanmaekelbergh, J. Meeldijk and S. G. Hickey, *Journal of the American Chemical Society*, 2006, **128**, 6792-6793.
21. J. E. Murphy, M. C. Beard, A. G. Norman, S. P. Ahrenkiel, J. C. Johnson, P. Yu, O. I. Micic, R. J. Ellingson and A. J. Nozik, *Journal of the American Chemical Society*, 2006, **128**, 3241-3247.
22. H. Zheng, R. K. Smith, Y.-w. Jun, C. Kisielowski, U. Dahmen and A. P. Alivisatos, *Science*, 2009, **324**, 1309-1312.
23. X. Wang and Y. Li, *Chemical Communications*, 2007, 2901-2910.
24. S. Ghosh, M. Roy and M. K. Naskar, *Crystal Growth & Design*, 2014, **14**, 2977-2984.
25. D. P. Singh, A. K. Ojha and O. N. Srivastava, *The Journal of Physical Chemistry C*, 2009, **113**, 3409-3418.
26. H. Xu, W. Wang, W. Zhu, L. Zhou and M. Ruan, *Crystal Growth and Design*, 2007, **7**, 2720-2724.
27. C. Yang, X. Su, F. Xiao, J. Jian and J. Wang, *Sensors and Actuators B: Chemical*, 2011, **158**, 299-303.
28. P. Akcora, H. Liu, S. K. Kumar, J. Moll, Y. Li, B. C. Benicewicz, L. S. Schadler, D. Acehan, A. Z. Panagiotopoulos and V. Pryamitsyn, *Nature materials*, 2009, **8**, 354-359.
29. E. Prodan and P. Nordlander, *The Journal of chemical physics*, 2004, **120**, 5444-5454.
30. Y. Yang, Q. Liao, J. Qi, W. Guo and Y. Zhang, *Phys. Chem. Chem. Phys.*, 2009, **12**, 552-555.
31. Z. Zhang, K. L. More, K. Sun, Z. Wu and W. Li, *Chemistry of Materials*, 2011, **23**, 1570-1577.
32. Y. Xu, D. Zhao, X. Zhang, W. Jin, P. Kashkarov and H. Zhang, *Physica E: Low-dimensional Systems and Nanostructures*, 2009, **41**, 806-811.
33. X. Li, H. Zhu, J. Wei, K. Wang, E. Xu, Z. Li and D. Wu, *Applied Physics A*, 2009, **97**, 341-344.
34. G. Du and G. Van Tendeloo, *Chemical Physics Letters*, 2004, **393**, 64-69.
35. S. Xiong, W. Qi, B. Huang, M. Wang and Y. Li, *Materials Chemistry and Physics*, 2010, **120**, 446-451.
36. S. Kar, B. N. Pal, S. Chaudhuri and D. Chakravorty, *The Journal of Physical Chemistry B*, 2006, **110**, 4605-4611.
37. L. Liao, H. Lu, J. Li, H. He, D. Wang, D. Fu, C. Liu and W. Zhang, *The Journal of Physical Chemistry C*, 2007, **111**, 1900-1903.
38. J. Chang, H. Kuo, I. Leu and M. Hon, *Sensors and actuators B: Chemical*, 2002, **84**, 258-264.
39. C. Wang, X. Fu, X. Xue, Y. Wang and T. Wang, *Nanotechnology*, 2007, **18**, 145506.